Gas-phase Perspective on the Thermodynamics and Kinetics of Heterogeneous Catalysis

Journal:	*Catalysis Science & Technology*
Manuscript ID:	CY-PER-04-2014-000435.R1
Article Type:	Perspective
Date Submitted by the Author:	28-May-2014
Complete List of Authors:	Armentrout, Peter; University of Utah, Chemistry

Gas-phase Perspective on the Thermodynamics and Kinetics of Heterogeneous Catalysis

P. B. Armentrout*[a]

Abstract

Studies of small gas-phase transition metal cluster cations (2 – 18 atoms) are reviewed with an emphasis on the thermodynamic information acquired. For the metal-metal bond energies, the cluster results deviate from the bulk-phase enthalpy of vaporization in a manner than can be quantitatively described by the spherical drop model that accounts for the surface free energy using bulk-phase parameters (within 10 – 20%). Binding energies of atomic H and O adsorbates to such clusters are found to vary extensively for the smallest clusters and to reach values lying close to bulk-phase adsorbate energies for all five metal systems that have been investigated (V, Cr, Fe, Co, and Ni). For molecular fragments (C, CH, CH_2, NH, and NH_2), binding energies to clusters are also found to plateau for larger clusters (greater than about 10 atoms). These asymptotic values may be useful in estimating such quantities on surfaces. In the case of atomic N adsorbates, variations in the adsorbate energies with cluster size remain appreciable through the size range studied, which appears to be a consequence of activating the very strong N_2 bond.

Introduction

Studies of heterogeneous catalysis are necessarily studies of surface science, and therefore accompanied by the myriad tasks of surface characterization, surface cleaning, surface poisoning, etc. However, given that many technologically important heterogeneous catalysts are dispersed metals, in part to enhance the surface area available for reaction, there is a growing need and interest in examining the chemistry of nanoscale particles. An interesting question arises concerning how small the surface can be and still be considered a surface. With the advent of nanotechnology and cluster studies involving a wide range of particle sizes, this question has begun to be answered, sometimes with surprising results. In many cases, the physical and chemical properties of cluster systems at the sub-nano and nanoscale differ from the bulk phase appreciably and can differ on an atom by atom basis. For example, supported iridium clusters show a dependence on cluster size in the hydrogenation of toluene[1] and nickel clusters supported on MgO exhibit size-dependent chemical reactivity towards CO dissociation.[2] CO oxidation by unsupported gold[3,4] and supported gold[5,6] and palladium[7] clusters also exhibit distinct size dependences. Perhaps more surprisingly, as will be recounted below, relatively small clusters, which are essentially all surface, can actually mimic some surface properties of the bulk phase with fidelity. Although not explicitly detailed below, this comparison also demonstrates that single metal atoms are generally distinct in their reactivity compared to surfaces, although myriad studies of such species attest to the utility of understanding atomic metal chemistry in other equally important environments (e.g., homogeneous catalysis and biological systems).[8-11]

Notably, because the means of experimentally exploring such pico-surfaces differ from those appropriate for the bulk phase, these gas-phase studies can provide information not otherwise readily accessible to condensed phase studies. In this review, quantitative work on transition metal clusters containing between two and eighteen atoms are recounted and the differences and similarities to bulk-phase surface properties explored. Because of the mass spectrometric methods used to isolate such clusters, it is known that they are completely clean (no adsorbates) with a well defined stoichiometry. This review will emphasize quantitative

thermodynamic information obtained from these studies, information that can permit an understanding and perhaps allow control of this interesting phase of matter. In addition, the thermodynamic data provided in these studies can act as benchmarks for theory, where calculations on metal clusters and surfaces are still challenging.

Experimental Methods

Instrumentation. Our cluster experiments utilize a guided ion beam tandem mass spectrometer (GIBMS), which has been described in the literature in detail.[12] Thermalized metal cluster cations are produced using a laser vaporization/supersonic expansion source,[13,14] in which the 511 and 578 nm radiation from an Oxford ACL 35 copper vapor laser is tightly focused onto a rod of the desired metal. The laser operates at 7 kHz with an optimum pulse energy of about 4 mJ. The metal rod, which is held by an aluminum source block, is continuously translated and rotated to provide fresh sample for ablation. A constant flow of about 6000 standard cm^3/min (sccm) of He entrains the vaporized metal and metal cations formed by laser ablation. As this mixture traverses a 2 mm diameter x 63 mm long condensation tube, collisions (about 10^5) and rapid mixing lead to the condensation of the metal into clusters and their thermalization, yielding a quasicontinuous beam of metal cluster cations. The initial laser plasma generates sufficient positive ions to act as seeds for condensation of metal cluster cations, such that no post-ionization (which might heat the ions) is required.

No direct measurements of the internal temperatures of the clusters are possible, but all studies to date suggest that the cluster cations generated are likely to be near room temperature.[12] In all of our work, we look for the possibility that isomers or excited electronic states of these species might be generated. Our methods are not sensitive to isomers or states having similar energies to the ground state but are very sensitive to such species (populations as little as ~0.1%) if that isomer or state lies greater than about 0.2 eV above the ground state. Evidence for such excited species is rare,[15-17] and none has been observed in our reactive studies. Overall, it appears that our source primarily produces thermalized species because the many low frequency

vibrational and rotational degrees of freedom available in these clusters allow efficient coupling between collisional (translational) and electronic degrees of freedom. If multiple low-lying isomers or states are present in our reactant cluster beams, they all have essentially the same energy within ~0.1 eV such that the thermochemistry measured is unaffected.

This seeded helium flow expands into vacuum, thereby undergoing a mild supersonic expansion. This first vacuum region is field free to avoid excitation of the clusters. The expansion is skimmed and passed through two differentially pumped regions before entering the primary mass spectrometer. Here, positively charged ions are accelerated and injected into a 60° magnetic sector momentum analyzer, where they are mass-selected with a resolution of better than a mass unit. The ions are then decelerated and focused into a radio frequency (rf) octopole ion guide[18-20] biased with dc and rf voltages. The latter establishes a potential that efficiently traps ions in the radial direction without influencing their kinetic energy. The dc potential allows accurate control of the translational energy of the ions in the guide, over a four order of magnitude range down to very low ion energies (<0.1 eV) and up through energies where chemical bonds can be made and broken. The octopole guide passes through a reaction cell containing the neutral reactant gas. The pressure of the neutral reactant gas is kept relatively low to reduce the probability of multiple collisions with the ions, but all studies are conducted at several neutral pressures (generally ~0.1 – 0.4 mTorr), such that only ~10% of the reactant ions undergo collisions at the maximum pressure. When necessary, the effects of multiple collisions are removed by extrapolating to zero pressure,

Absolute cross sections. After passing through the reactant cell, remaining reactant and newly formed product ions drift to the end of the octopole. Here, they are extracted, injected into a quadrupole mass filter for mass analysis, and their intensities measured with a Daly detector (which utilizes a 28 kV conversion dynode to ensure good sensitivity over a wide mass range)[21] coupled with standard pulse counting techniques. Reactant ion intensities generally range from $10^5 - 10^6$ ions/s. Because the pressure of the neutral gas and the length of the interaction region are known, reactant and product ion intensities can be converted to absolute reaction cross

sections, $\sigma(E)$, using a Beer's law approach, as discussed in detail elsewhere.[19] Absolute errors in the cross sections are on the order of ± 30%. For comparison to other experiments conducted at thermal energies, rate coefficients, $k(E)$, can be derived simply by multiplying by the velocity, i.e., $k(E) = v\ \sigma(E)$ for cross sections measured at the lowest energies. Averaging these microcanonical rate coefficients over a Maxwell-Boltzmann distribution then recovers $k(T)$.

Energy scale. The nominal kinetic energy of the reactant ions when undergoing collision with the reactant neutral is given by the dc voltage applied to the octopole guide relative to the voltage where the reactant metal cluster cations are generated. To determine the absolute zero in the kinetic energy of the ions, the octopole is used as a retarding energy analyzer,[19] in which the dc voltage is swept through the nominal energy zero. Because only ions having forward velocities are transmitted, this cutoff curve can be differentiated and the resultant peak fit with a Gaussian distribution to determine both the absolute energy zero and the energy distribution of the reactant ions. The latter (full width at half maximum) is generally 0.5 – 2.0 eV, gradually increasing with cluster size. This process has an uncertainty in the zero of the absolute energy scale of 0.05 eV in the lab frame. Because a certain fraction of the laboratory kinetic energy must be conserved (a result of conservation of linear momentum of the reacting system through the laboratory), the kinetic energies in the laboratory frame are converted to center-of-mass (CM) energies using the stationary target approximation, $E(\mathrm{CM}) = E(\mathrm{lab})\ m/(m + M)$ where m and M are the masses of the neutral and ionic reactants, respectively. The center-of-mass frame energies correspond to the energy available to the reaction system. In addition, the distribution of kinetic energies is corrected for its truncation at the lowest energies.[19]

Energy Dependence of Exothermic Reactions. Because of the long-range attractive interactions between ions and polar or polarizable molecules, exothermic ion-molecule reactions often occur at the collision rate. For polarizable molecules, this is described using the Langevin-Gioumousis-Stevenson (LGS) expression,[22] $\sigma(E) = \pi\ q\ (2\alpha / E)^{1/2} = 16.859\ \text{Å}^2\ (\alpha/E)^{1/2}$, where E is the collision energy in the CM frame (in eV), q is the charge on the ion (in C), and α is the polarizability volume of the neutral (in Å^3). Thus, the cross section declines as $E^{-1/2}$ as the

energy increases, eventually reaching the hard-sphere collision limit at higher energies. Note that the LGS expression leads to rate coefficients, $k(E)$ or $k(T)$, that are independent of energy and therefore temperature, as has been observed for many ion-molecule reactions. Polar molecules enhance the collision cross section further, but require more complicated expressions because of the angular dependence of the dipole moment towards the ion.[23]

Energy Dependence of Endothermic Reactions. There is no single model that rigorously describes the kinetic energy dependences of cross sections for endothermic processes. In our work, we use a modified line-of-centers model, eqn (1),

$$\sigma(E) = \sigma_0 (E - E_0)^N / E \qquad (1)$$

where σ_0 is an energy independent scaling parameter, E is the relative kinetic energy, E_0 is the threshold for reaction at 0 K, and N characterizes how the available energy is utilized by the reacting system.[24] When $N = 1$, eqn (1) corresponds to the line-of-centers model for collisions of hard spheres, which rigorously conserves angular momentum, whereas $N = 1/2$ yields a form that is the microscopic reverse of the LGS expression.[25,26] The form of the cross section in eqn (1) leads to an Arrhenius-like expression when converted to $k(T)$. The utility of eqn (1) has been demonstrated upon many occasions, but its application to real systems requires consideration of several experimental parameters. Chief among these is explicitly including the distributions of kinetic and internal energies of the reactants. The convolution over the kinetic energy distributions is described elsewhere.[19] Internal energies are included by summing over the rovibrational states of the clusters having energies E_i and populations g_i, where $\Sigma g_i = 1$, eqn (2).

$$\sigma(E) = \sigma_0 \sum_i g_i (E + E_i - E_0)^N / E \qquad (2)$$

Vibrational frequencies for the bare metal clusters are obtained by using an elastic cluster model suggested by Shvartsburg *et al*.[27]

We also consider whether the reaction of interest will occur during the time available, i.e., the flight time of the ions from the collision cell to the quadrupole mass filter, τ, which is approximately 100 μs in this apparatus. This effect becomes increasingly important as the size

of the cluster increases,[15] because metal clusters have many low frequency vibrational modes, such that the lifetime of the transient intermediate increases with cluster size, eventually exceeding τ. To include this effect, eqn (2) is converted to eqn (3),[28-32]

$$\sigma(E) = (N\sigma_0 / E)\sum_i g_i \int_{E_0 - E_i}^{E} [1 - e^{-k(E^*)\tau}] \, (E - \varepsilon)^{N-1} d\varepsilon \qquad (3)$$

where ε is the energy transferred from the reactants' kinetic energy into internal energy of the energized molecule (EM) during the collision. The term in square brackets represents the probability for reaction and relies on the unimolecular rate coefficient for dissociation, $k(E^*)$, where E^* is the internal energy of the EM after the collision, i.e., $E^* = \varepsilon + E_i$.[30] Note that if this probability is unity, then the integration of eqn (3) recovers eqn (2). $k(E^*)$ is calculated using statistical Rice-Ramsperger-Kassel-Marcus (RRKM) theory,[33-35] as shown in eqn (4),

$$k\ (E^*) = d\ N_{vr}^{\dagger}(E^* - E_0) / h\rho_{vr}(E^*) \qquad (4)$$

where d is the reaction degeneracy; h is Planck's constant; $N_{vr}^{\dagger}(E^* - E_0)$ is the sum of the rovibrational states of the transition state (TS) at an energy $E^* - E_0$; and $\rho_{vr}(E^*)$ is the density of rovibrational states of the EM at the available energy, E^*. Extensions of these models to competitive reactions, sequential reactions, and association reactions, all treated statistically, have also been made.[36-38]

Because transition metal clusters have an appreciable density of electronic states, the use of RRKM theory may not be entirely appropriate.[12] However, we use this model because there are no reliable means of accurately estimating the density of electronic states and more appropriate models are not yet available. Because reactants and products share this high density of electronic states, the errors associated with neglecting the electronic state density should largely cancel.

In our studies, we extract thermodynamic information by using eqn (3) to analyze the experimental kinetic energy dependent cross sections. This comparison requires that the model cross section is convoluted with the kinetic energy distributions of the ion and neutral reactants, as noted above.[19] The parameters σ_0, N, and E_0 are adjusted until the data are reproduced over

extended ranges of energy and magnitude. Uncertainties in the derived E_0 values include errors associated with variations in E_0 over the range of N values that adequately reproduce several data sets, variations in the vibrational frequencies of the reactant cluster ions, energized molecules, and transition states, variations in the time scale available to the reaction, and the absolute uncertainty in the energy scale. Thus, the uncertainties include all known random and systematic uncertainties in the data acquisition and analysis.

Stabilities of Bare Metal Cluster Cations

In order to understand the reactivity on metal cluster surfaces, the stability of those surfaces must first be established. In the gas phase, the decomposition of the surface (generally by emission of atoms) is a viable pathway at some of the elevated energies examined in these studies. The propensity for this reaction is easily quantified by using an unreactive neutral reagent. In all our work, this has been the rare gas Xe, which is chosen because its relatively large polarizability enhances the efficiency of kinetic to internal energy transfer in any collision event.[39,40] Thus, we use GIBMS to examine the kinetic energy dependence of collision-induced dissociation (CID), reaction (5).

$$M_n^+ + Xe \rightarrow M_{n-1}^+ + M + Xe \qquad (5)$$

It is also feasible for the clusters to dissociate not by the "evaporation" reaction (5), but by "fission" yielding two smaller clusters, reaction (6).

$$M_n^+ + Xe \rightarrow M_{n-m}^+ + M_m + Xe \qquad (6)$$

Interestingly, reaction (6) is clearly favored thermodynamically over loss of multiple M atoms, although it is entropically disfavored because the collective motions of the m atoms during dissociation must be much more organized. The latter effect dominates such that the fission process is a relatively rare event, having only been observed for V_4^+ (dominant), V_n^+ where n = 5, 7, 9, 11, 13, 14, 15 (minor), Cr_5^+ (dominant), Cr_6^+ (minor), Ni_5^+ (minor), Nb_4^+ (dominant), and Nb_n^+ where n = 5 – 11 (minor). In each of these cases, the only neutral cluster formed is the dimer (m = 2). Thus, fission can compete with evaporation in cases where the neutral dimer bond is

particularly strong (V and Nb) or when the cationic cluster bond energy for M_{n-1}^+ is particularly weak. Examples of both evaporation and fission are shown in Figure 1, which compares dissociation of the tetramer cations of Ti and V. For Ti_4^+, the sequential loss of atoms is apparent, whereas for V_4^+, it can be seen that the V_2^+ product not only has a lower threshold than V_3^+ but two features are evident, clearly corresponding to formation of $V_2^+ + V_2$ (fission) and $V_2^+ + 2$ V (evaporation).

Because there is a long-range attractive interaction between the products of reactions (5) and (6), no barriers in excess of the endothermicity of these CID processes are expected, such that the E_0 value measured by analyzing the data with eqn (3) equals the bond dissociation energy (BDE) of interest, $D(M_{n-1}^+-M)$ for reaction (5) and $D(M_{n-2}^+-M_2)$ for reaction (6). Such studies in our laboratory now include measurements for most of the first-row transition metal clusters, Ti_n^+ (n = 2 - 22),[16] V_n^+ (n = 2 - 20),[41] Cr_n^+ (n = 2 - 21),[42,43] Mn_2^+,[44,45] Fe_n^+ (n = 2 - 19),[12,15,46] Co_n^+ (n = 2 - 18),[17,40] Ni_n^+ (n = 2 - 18),[47,48] and Cu_2^+,[49] along with the second-row transition metal clusters of Nb_n^+ (n = 2 - 11),[50,51] and the third row transition metal clusters of Ta_n^+ (n = 2 - 4).[52] These results are reviewed thoroughly elsewhere.[53-55]

It is also worth noting that ionization energies (IEs) of the neutral clusters have been measured by others for vanadium,[56,57] chromium,[58] iron,[59-62] cobalt,[59,62] nickel,[62,63] and niobium.[64] The thermodynamic cycle of eqn (7) can be used to combine these IE values with our cationic BDEs to yield neutral BDEs.

$$D(M_{n-1}-M) = D(M_{n-1}^+-M) + IE(M_n) - IE(M_{n-1}) \quad (7)$$

Such results have been reviewed elsewhere and generally follow the same trends observed for the cationic clusters.[53-55]

Figure 2 shows the cationic results for the three early first-row transition metals, Ti, V, and Cr. It can be seen that there are variations in the stability of the clusters with their size and that the patterns differ from metal to metal. In the case of Cr, there is a pronounced even-odd alternation in the BDEs for the smallest cluster cations. This can be attributed to the stable half-filled shells of the $Cr(^6S, 4s^1 3d^5)$ ground state combining with the $Cr^+(^5S, 3d^5)$ ground state. Here, cationic clusters

having an odd number of Cr atoms have an even number of 4s valence electrons, which pair leading to enhanced stability. Vanadium shows exactly the opposite effect, with even-sized cluster cations being more stable compared to the odd-sized clusters. In this case, ground state $V^+(^5D, 3d^4)$ can combine with ground state $V(^4F, 4s^2 3d^3)$ to form a strongly bound dimer. Larger clusters then grow by addition of $V(^6D, 4s^1 3d^4)$, such that the stable clusters are again those having an even number of 4s valence electrons. In contrast, titanium shows no strong even-odd oscillations but rather the most stable structures lie at n = 7, 13, and 19. This pattern has been attributed to icosahedral-like packing, such that these clusters are postulated to have pentagonal bypyramid, icosahedral, and double icosahedral structures, respectively. Of course, the pentagonal symmetry of these structures cannot extend completely to the bulk phase. Nearly all metal cluster cations we have examined show that the n = 13 cluster is particularly strongly bound, often accompanied by n = 6 and 15, as exhibited by V_n^+. This pattern is more suggestive of octahedral symmetry, in which the 13-mers would be a face-centered cubic (fcc) cubooctahedron and the 15-mers would be body-centered cubic (bcc) rhombic dodecahedrons. Such suggestions were initially forwarded on the basis of chemisorption results of Parks et al.[65] for iron clusters.

It is clearly of interest to examine how the BDEs of these small cluster cations are related to the bulk phase properties of these metals. This relationship can be examined using the cohesive energy, $E_c(n)$, defined as the atomization energy of the cluster (i.e., the sum of the BDEs) normalized by n. The cohesive energies of six first-row transition metal cluster cations along with niobium from the second-row are shown in Figure 3, normalized by their bulk phase heats of vaporization plotted versus $n^{-1/3}$, which should be related to the surface area of the cluster. It can be seen that these cohesive energies all extrapolate towards $\Delta_{vap}H_0$, the bulk phase heat of vaporization, especially once the value of n exceeds 3 or 4. Indeed a linear regression of these points yields intercepts within 10% of the $\Delta_{vap}H_0$ values, which vary considerably, from 4.1 eV for Cr to 7.6 eV for Nb.[53,55] Thus, the BDEs of the various metals properly reflect the different bulk-phase vaporization energies. The reason that the clusters have much lower cohesive

energies than the bulk can be related to the surface energy of the cluster. This relationship has been described using the "spherical drop" model of Miedema,[66,67] eqn (8),

$$E_c(n) = \Delta_{vap}H_0 - (36\pi/n)^{1/3}\,\gamma^\circ\,V_a^{2/3} \qquad (8)$$

where γ° is the surface free energy of the bulk metal and V_a is the atomic volume in the bulk. The three lines in Figure 4 show the predictions of this model using the bulk phase values for iron ($\Delta_{vap}H_0$ = 4.28 eV, $\gamma^\circ = 1.6 \times 10^{19}$ eV/m^2, and $V_a = 1.18 \times 10^{-29}$ m^3),[66,67] nickel ($\Delta_{vap}H_0$ = 4.44 eV, $\gamma^\circ = 1.53 \times 10^{19}$ eV/m^2, and $V_a = 1.09 \times 10^{-29}$ m^3), and niobium ($\Delta_{vap}H_0$ = 7.60 eV, $\gamma^\circ = 1.7 \times 10^{19}$ eV/m^2, and $V_a = 1.8 \times 10^{-29}$ m^3), the metals having the largest and smallest (Ni for first-row metals and Nb overall) predicted slopes, $(36\pi V_a^2)^{1/3}\,\gamma^\circ/\Delta_{vap}H_0$. It can be seen that the data for four of the metals fall nicely inside the predicted band, clearly indicating that the bulk-phase surface energy explains the deviations from the bulk. Even including the outliers, the slopes of these lines for the seven different elements differ by only 18 ± 9% from the bulk phase values suggested by Miedema,[66,67] thus much of the deviations observed are within the experimental uncertainties. Additional deviations from the predictions using bulk phase values can be understood if these very small clusters have surface areas larger than a smooth sphere, which seems likely for these atomic scale clusters.

Similar data has been obtained for the cohesive energies of neutral transition metal clusters. Again extrapolation to the bulk limit gives intercepts, $\Delta_{vap}H_0$ values, within 10% of the bulk phase values.[53,55] Now, the slopes of these lines differ from the bulk phase values by an average of 41 ± 11%. The difference between the cationic and neutral clusters may simply reflect the smaller volume resulting from contraction of the electron orbitals with increased nuclear charge.

Overall, comparisons to the spherical drop model show that the properties of the transition metals that control the binding energies of small clusters are the same properties that control the bulk phase thermodynamic stabilities, both for cationic and neutral clusters. However, even though the cluster stabilities extrapolate smoothly to the bulk phase, the largest clusters examined here ($n \sim 20$) have cohesive energies of only 60 – 70% of the bulk phase value. This is clearly

because clusters comprise nearly all surface atoms. This observation is important in understanding the results for adsorbate interaction energies discussed below.

Reactivity Studies

Thermochemistry of simple adsorbates to metal cluster cations can be acquired by examining the kinetic energy dependence of the bimolecular reactions (9) – (11).

$$M_n^+ + RL \rightarrow M_nL^+ + R \quad (9)$$

$$M_{n+1}^+ + RL \rightarrow M_nL^+ + M + R \quad (10)$$

$$M_{n+x}^+ + RL \rightarrow M_nRL^+ + x\,M \quad (11)$$

Our studies have included adsorbates such as oxygen (L = O, RL = O_2, CO_2), hydrogen (L = H, RL = H_2, CH_4, NH_3), nitrogen (L = N, RL = N_2, NH_3), hydrocarbons (L = CH_y, y = 0 – 3, RL = CH_4), and nitrogen-based ligands (L = NH_y, y = 0 – 2, RL = NH_3). Using the methods outlined above, the kinetic energy dependent cross sections for such reactions are analyzed to yield the reaction threshold, E_0. These threshold energies are converted to bond energies of interest, $D(M_n^+ - L)$, as outlined in eqns (12) – (14).

$$D(M_n^+ - L) = D(R - L) - E_0(9) \quad (12)$$

$$= D(R - L) + D(M_n^+ - M) - E_0(10) \quad (13)$$

$$D(M_n^+ - R,L) = D(R - L) + D(M_n^+ - xM) - E_0(11) \quad (14)$$

Thus, the previous determination of the bare cluster stabilities allows the latter two reactions to be used for additional thermochemical studies. Results from these reactivity studies have been reviewed elsewhere.[55,68,69]

Oxidation of Transition Metal Cluster Cations and M_n^+–O Bond Energies

The kinetic energy dependence of reactions of metal cluster cations with O_2 has been studied for V_n^+ (n = 2 - 17), Cr_n^+ (n = 2 - 18), Fe_n^+ (n = 2 - 18), Co_n^+ (n = 2 - 20), and Ni_n^+ (n = 2 - 18).[70-74] Most transition metal cluster cations (as well as neutrals) react with O_2 efficiently to form a cluster dioxide, reaction (11). The reaction efficiencies approach 100% of the collision

cross section and rapidly reach the hard-sphere limit, as shown for the example of V_{10}^+ in Figure 4. The overall reaction is clearly exothermic and barrierless as the total cross section increases as low in energy as examined. The excess energy from the oxidation process leads to expulsion of M atoms from the initially formed $M_nO_2^+$, which immediately verifies that M–O bonds are stronger than M–M bonds. The number of M atoms lost (x) is determined by the overall reaction exothermicity and the initial cluster size. Larger clusters can dissipate the exothermicity among more degrees of freedom, such that the kinetics for expulsion of M atoms slows down. For the largest clusters examined, the $M_nO_2^+$ adduct can be observed at the lowest collision energies, with dissociation by metal atom loss occurring as the collision energy is increased. Monoxide product ions, M_mO^+, are also observed and can result from either loss of an oxygen atom or loss of MO. The latter channel is only observed for the early metals, as these have strong MO bond energies. Thus, in Figure 4, the low energy (exothermic) feature in V_9O^+ results from VO formation, whereas the higher energy (endothermic) feature can be attributed to V atom loss from the $V_{10}O^+$ product formed by O atom loss. The other V_mO^+ products are then formed by sequential V atom loss from each of the primary products. This demonstrates that $D(M_n^+–O) > D(M_{n-1}^+–M)$, which also means that formation of M_nO^+ products generally has a smaller cross section than the $M_mO_2^+$ dioxides. For most systems, the IEs of M_mO_2 and M_mO products are lower than those of M and MO, such that $M_mO_2^+$ and M_mO^+ are usually the product ions observed and rarely M^+ or MO^+. For small clusters, alternative pathways can also be seen occasionally, e.g., formation of $M_{n-1}^+ + MO_2$.

Because the formation of the primary products is exothermic in these systems, no thermochemistry (other than a limit) can be ascertained from these reactions. Rather, by analyzing the thresholds for the endothermic formation of the smaller $M_mO_2^+$, the BDEs for M_m^+-2O can be determined. For the monoxides, thresholds for formation of the primary $M_nO^+ +$ O product channels do *not* yield accurate thermochemistry because this reaction competes with the much more favorable formation of the $M_mO_2^+$ products. However, the thresholds for higher order monoxide products ($M_{n-1}O^+$, etc.) do yield reasonable thermochemistry.[70-74] This is

verified from threshold measurements for reactions of chromium (n = 2 – 18) and iron (n = 2 – 18) cluster cations with CO_2,[75,76] which is a good donor of a single oxygen atom (because the CO molecule is a good leaving group). We find that the M_n^+-O BDEs are comparable to half the M_n^+-2O BDEs for all metals once the clusters get large enough (about four atoms or so).[70-74] Because these various measurements are completely independent, such agreement validates their accuracy. Perhaps not surprisingly, the equivalent BDEs indicate that the first and second oxygen atom can find similar binding sites on all but the smallest clusters.

Quantitative comparison of M_n^+-O BDEs with the M_n^+-M BDEs shows that the former are much larger than the latter, in agreement with the qualitative behavior of the reaction cross sections. Indeed, the M_n^+-O BDEs exceed the M_n^+-M BDEs by more than 1 eV with the exception of the atoms (n = 1) of Fe, Co, and Ni. Figure 5 shows the cluster oxide BDEs normalized to bulk phase oxygen atom adsorbate energies, which vary considerably with metal identity: 6.3, 6.5, 5.4, 5.0, and 4.9 eV for V, Cr, Fe, Co, and Ni surfaces, respectively.[77] The first four of these values are estimated from the enthalpies of formation of bulk compounds and only the latter value has been measured directly. Similar values have been obtained from calorimetry experiments:[78-85] 6.3 ± 0.2 eV for Cr, 4.0 – 5.5 eV for Fe, 4.7 – 5.1 for Co, and 5.0 and 4.8 eV for Ni(111), 5.0 eV for Ni(110), and 5.4 eV for Ni(100). As a function of cluster size, vanadium behaves somewhat differently than the other metals by reaching a maximum BDE at n = 5, and then declining to a plateau above n = 10. For iron, variations in cluster-oxide BDEs persist to relatively high values of n. In general though, the cluster oxide BDEs reach nearly constant values for clusters above about n = 10 (and down to n = 5 for Cr, Co, and Ni), Figure 5. These asymptotic values are within 10% of the bulk phase oxygen adsorbate energy for all metals, even though the latter differ by over 30%. Thus, the cluster BDEs properly reflect the strong changes in oxygen binding observed with the identity of the metal. It is perhaps surprising that this near bulk-phase limit is reached even for very relatively small clusters, in several cases, down to about n = 5. This plateau behavior is believed to be a direct result of the very strong M_n^+–O bonds, which can clearly disrupt the metal-metal bonding, thereby annealing the cluster oxide

complexes. This presumably allows rearrangement of the cluster to enable formation of the strongest possible cluster bond to oxygen.

Overall, these observations are in direct contrast to those for the approach to bulk phase behavior for the bare metal clusters, where the largest clusters have cohesive energies that are only 70% of the bulk phase limit, Figure 3. In contrast, oxygen atom adsorbates interact with metal clusters with energies near the bulk phase limit even for relatively small clusters. We believe this is a consequence of comparing a surface phenomenon (oxygen adsorption) with the more bulk phase metal-metal binding. Clearly, any adsorbate can only bind to one, two, three, perhaps four metal atoms on a surface, sites that are easily reproduced even on small clusters. Because the strength of this interaction depends on the ability of the metal (whether in the bulk or in a cluster) to move electron density to form a bond, even a modest sized metal cluster has sufficient electronic flexibility to form as strong a surface-adsorbate bond as the bulk. In essence, it appears that chemical bonding to a metal surface is a more local phenomenon than properties such as ionization energies, electron affinities (the work function of the bulk), and vaporization energies.

In addition to these studies of the binding of one and two oxygen atoms to clusters, it is also possible to create more heavily oxidized clusters directly in the source (by introduction of O_2 into the He flow). Using this method, we have generated species like $Fe_nO_m^+$ where n = 1 – 10 and m encompasses 3 – 9 values for each n value. Quantitative evaluation of these species is presently limited to CID of the iron oxide cation clusters where n = 1 – 3.[86] Because many of the dissociation pathways observed include intact iron oxide neutrals (e.g., FeO, FeO_2, Fe_2O_2, Fe_2O_3), the data acquired leads to thermochemistry for both cationic and neutral clusters. When these data are examined as a function of the oxidation state of the metal, it becomes clear that the clusters with the strongest cluster-oxide bonds have oxidation states near 2, dropping off both to lower and higher oxidation states. This is consistent with our observations that the $n = m$ cationic clusters are often the most stable stoichiometry generated in our source. One potentially

intriguing aspect of continued studies of such species is the control over the oxidation state in the cluster, which is unavailable using stable bulk phase stoichiometries.

Hydrogenation of Transition Metal Cluster Cations and M_n^+-H Bond Energies

The kinetic energy dependence of reactions of metal cluster cations with dihydrogen have been studied with V_n^+ (n = 2 - 13), Cr_n^+ (n = 2 - 14), Fe_n^+ (n = 2 - 15), Co_n^+ (n = 2 - 16), and Ni_n^+ (n = 2 - 16).[69-73] Unlike the exothermic oxidation reactions with O_2, hydrogenation of metal cluster cations in the reactions with dihydrogen is generally endothermic. (In all our studies, reactions are conducted with D_2 as this provides much more efficient mass separation between the reactant and product ions. As zero point energies differences between H and D bonds should be no more than 0.03 eV, the thermochemistry is largely unaffected.) This simply reflects the fact that the cluster hydride bond energy is weaker than the H_2 bond energy. As a consequence, the primary reaction observed with D_2 is endothermic formation of $M_nD^+ + D$, which has a cross section that reaches a maximum at higher energies when the product ion dissociates to $M_n^+ + D$. This is shown for the example of V_{10}^+ in Figure 6. No $M_{n-1}D^+$ products are ever observed, indicating that the metal-metal bonds are stronger than the metal-hydride bonds. The peak in the M_nD^+ cross section corresponds well to the $D_0(D_2)$ bond energy (the thermodynamic onset for the dissociation process) for small clusters, but moves to higher energies for larger clusters, which reflects their extended lifetime. The extended lifetimes of larger clusters is also exhibited by the observation of $M_nD_2^+$ products, which are only observed for $n \geq 6$ for V (Figure 6), $n \geq 5$ for Cr, $n \geq 9$ for Fe, n = 4, 5, and ≥ 9 for Co, and $n \geq 5$ for Ni. $M_nD_2^+$ formation is not observed for smaller clusters because the lifetime of the $M_nD_2^+$ complex is too short to observe experimentally. In many cases, formation of $M_nD_2^+$ products requires overcoming a barrier (Figure 6), indicating that the species formed is dissociatively chemisorbed D_2. Chemisorption is also suggested by calculations that the lifetimes of physisorbed $M_n(D_2)^+$ adducts are much shorter than the experimental time available for dissociation back to reactants (~10^{-4} s) such that such physisorbed adducts would not be observed. In a few cases, the formation of $M_nD_2^+$ is

unactivated: Cr_n^+ (n = 6 – 8), Fe_9^+, Co_n^+ (n = 4, 5, ≥ 10), and Ni_n^+ (n ≥ 5). In these cases, the barrier between the physisorption and chemisorptions wells lies below the reactant asymptotic energy.

Analysis of the cross sections for M_nD^+ formation allows the determination of M_n^+-D BDEs, as collected in Figure 7. Most M_n^+-D BDEs show sharp variations for smaller clusters, which reflects the evolution of their electronic and geometric structures. Note that iron is the only metal for which the M^+–D bond is stronger than the M_2^+–D bond, which is because Fe^+ is the only metal studied that has a 4s electron in its ground electronic state, Fe^+ ($^6D,4s^13d^6$), such that FeD^+ is an even valence electron species and Fe_2D^+ has an odd number of valence electrons. As the clusters get larger, the BDEs for all metals approach the bulk-phase value. (For H atom adsorption, the bulk phase adsorbate energies are confined to a fairly narrow range with values of 2.66 ± 0.08 eV for V(100),[87,88] ~3.21 eV for polycrystalline Cr,[78,89] 2.80 ± 0.10 eV for Fe(100), Fe(110), and Fe(111),[77,90,91] 2.60 eV for Co(0001) and 2.65 eV for to Co(1010),[92,93] and 2.70[94] and 2.74 eV on Ni(111),[95,96] 2.74 eV on Ni(100),[95] and 2.70 eV on Ni(110).[95]) Indeed, for V, Fe, Co, and Ni, M_n^+–D BDEs for n > 10 are all within 10% of the bulk-phase limit. For Cr, it is clear that the evolution towards the bulk is developing more slowly, but the trend is nevertheless apparent.

It is instructive to compare the M_n^+-D with the M_n^+-M BDEs. For chromium, the two show the same even-odd alternation, consistent with the similar valence electronic structure of D atoms, $^2S(1s^1)$, and Cr atoms, $^7S(4s^13d^5)$. In addition, the values are fairly similar throughout the range studied (average difference of 0.16 ± 0.13 eV, with the exception of n = 2 and 3 where the deuteride bonds are ~0.8 eV stronger), suggesting that the stable, half-filled 3d shell of chromium is not particularly active in the metal-metal bonding. On the other hand, the V_n^+-D and V_n^+-V BDEs parallel one another for n ≥ 5, but the deuteride values are lower than the metal-metal values by an average of 1.5 ± 0.2 eV. Thus, V_n^+-V bonding must include contributions from both 4s-4s and 3d-3d interactions. Likewise, the iron, cobalt, and nickel systems generally have stronger M_n^+-M BDEs than M_n^+-D BDEs. The average differences are 0.30 ± 0.07 eV for

iron with n = 2 – 4, 6, 7, 9, 10, 13 and 15; 0.66 ± 0.10 eV for Co with n = 1, 4, 6, 8 – 10, and 13; and 0.56 ± 0.10 eV for Ni with n = 5, 6, 8 – 11, and 14 – 16. These increases must again be attributed to 3d-3d interactions in the metal-metal bonds, although they are not as strong as the difference for vanadium (presumably because only 3d-3d bonding orbitals are occupied for the early metal where the d shell is less than half filled). However, some clusters (particularly n = 12 for Fe, Co, and Ni, and n = 5 and 14 for Fe and Co) have metal-metal BDEs that are much stronger than the metal-deuteride BDEs. In these cases, the M_{n+1}^+ clusters can have a highly symmetric geometrical structure compared to neighboring clusters: M_6^+ (octahedral), M_{13}^+ (icosahedral or octahedral with fcc or bcc packing), and M_{15}^+ (bcc rhombic dodecahedral). Thus, substitution of D for M in these clusters breaks the symmetry, changing the molecular orbital ordering, and apparently leads to weaker binding.

Activation of the Strong N_2 Bond

Because the N_2 bond is very strong, 9.76 eV, reactions of metal cluster cations M_n^+ with dinitrogen lead mainly to collision-induced dissociation, i.e., loss of metal atoms in reaction (5). Activation of the N_2 bond accounts for only a minority of products,[97,98] but these include formation of both mononitride and dinitride cluster ions, M_mN^+ and $M_mN_2^+$, where $m \leq n$. Both products dissociate by loss of additional metal atoms as the energy is increased, demonstrating that M_n^+-N BDEs exceed M_n^+-M BDEs and that the $M_mN_2^+$ species must be a dinitride, not a physisorbed N_2 complex. This latter conclusion is also demonstrated by the observation that $M_mN_2^+$ formation is an activated process, requiring considerable energy, whereas physisorption of an intact N_2 molecule should require no activation energy. Variations in the largest value of m observed for the product $M_mN_2^+$ from a particular reactant n show that the lifetime of the product ions increases with the size of the cluster. Thus, smaller M_n^+ clusters react with N_2 to form a complex that must lose two metal atoms in order to stabilize the $M_{n-2}N_2^+$ product species observed, whereas larger reactant clusters form complexes having sufficiently long lifetimes that $M_{n-1}N_2^+$ is observed, and the largest M_n^+ reactants allow $M_nN_2^+$ to be observed.

The analysis of these cross sections is complicated by the competition between the mononitride and dinitride product ions, however, reasonable results appear to be obtained when this competition is explicitly accounted for. Figure 8 shows the thermodynamic results for the M_n^+–N BDEs scaled by the bulk-phase adsorption energies of 5.7 eV for Fe (a reinterpretation of the work of Boszo et al.[90,91] by Stoltze and Nørskov[99]) and 7.24 eV for Co.[77] (This value for Co has been estimated from the enthalpies of formation of bulk cobalt nitrides and is substantially higher than for Fe and Ni, which are both near 6 eV. It seems possible that our average Co_n^+–N BDE value of 6.3 ± 0.2 eV is a more accurate estimate of the true bulk phase adsorption energy.) Values for the two metals are similar once scaled (for either scaling factor), indicating that the cluster values again reflect the large difference in bulk-phase thermochemistry. Values obtained from interpretation of the thresholds for generation of $Fe_{n-x}N_2^+$ yield somewhat lower values (not shown), indicating that the second nitrogen atom binds somewhat less strongly to the clusters. Figure 8 shows that the cluster values have not reached an asymptotic value, as they did for O and D, however, the strongest cluster BDEs do give values comparable to the bulk phase. This difference in behavior is believed to be a consequence of the very strong N_2 bond, which means that its cleavage is an activated process whereas cleavage of O_2 is unactivated and cleavage of D_2 is either unactivated or has only a small barrier. When the process is strongly activated, only a small fraction of the reactants lead to formation of the initial $M_nN_2^+$ intermediate, which makes the reaction much more sensitive to the details of the electronic and geometric structure of the reactant cluster. In contrast, an unactivated process allows the M_n^+-X_2 (X = O and D) adsorption energy to anneal the intermediate and find more stable products, leading to more efficient reaction.

In these systems, it was also possible to obtain thresholds for formation of the $M_nN_2^+$ products for the largest cluster cations. These analyses yield consistent thresholds for all clusters exhibiting this reaction with average values for E_0 of 0.48 ± 0.03 eV for iron and 0.78 ± 0.12 eV for cobalt. The former value agrees well with an estimate for the activation barrier for dinitrogen dissociation on Fe surfaces being greater than 0.4 ± 0.05 eV.[77] The fact that the activation

energy is higher on cobalt clusters is consistent with cobalt being a less active catalyst for ammonia synthesis in the Haber-Bosch process.

Methane Activation and Bond Energies to Hydrocarbon Radicals

Metal cluster cations of iron, cobalt, and nickel react with methane to gradually disassemble the methane molecule forming metal cluster cations bound to hydride (H), methyl (CH_3), methylene (CH_2), methylidyne (CH), and carbide (C) fragments.[100-102] (As for reactions with dihydrogen, our methane studies are conducted using perdeuterated methane. Again the thermochemistry should be unaffected except for the small zero point energy differences.) At low energies, the primary product formed is the dehydrogenation product, $M_nCD_2^+$, because the stable D_2 molecule is also produced. Although $M_nCD_3^+$ products are observed for a few clusters, these products generally dehydrogenate efficiently leading to rapid formation of M_nCD^+. At the highest collision energies, M_nD^+ and M_nC^+ are the dominant products, consistent with the formation of carbide layers on most bulk surfaces. For all products, thresholds are observed, indicating that reaction with methane on these metal cluster cations is an activated process. This is consistent with observations on the analogous bulk phase metal surfaces. Although not observed on nickel, the largest iron and cobalt clusters, $n \geq 10$, also form the $M_nCD_4^+$ product. This species is not observed for smaller clusters because the lifetime for dissociation back to reactants is too short.

Cluster BDEs to D, C, CD, and CD_2 are again determined using the analysis tools described above. In most cases, the $M_nCD_y^+$ product ions dissociate by losing metal atoms, such that threshold energies for formation of both the primary reaction (9) and secondary reaction (10) can be determined with the values providing an internal check on the thermochemistry derived. For the cases of D, C, and CD, the BDEs determined by analyses of these primary and secondary reactions agree with one another within experimental error for Fe, Co, and Ni clusters and the M_nD^+ BDEs are consistent with those obtained from reactions with D_2.[103-105] In contrast, the $Fe_nCD_2^+$ BDEs obtained from analyses of the primary reactions are much lower than those derived

from analyzing the secondary reactions (except for n = 3 and 4) and a similar observation is made for several $Co_nCD_2^+$ species. For the iron system, the M_n^+–CD_2 BDEs derived from the secondary reactions are 0.7 ± 0.3 eV greater than those from the primary reaction, and a similar difference of 0.7 ± 0.2 eV is found for Co_n^+ (n = 3 and 4). (The secondary reaction is not observed for Co_n^+ where $n \geq 5$ or for any Ni_n^+. In these cases, no comparable thermodynamic information could be obtained, although for nickel cluster cations, there are reasons to believe the primary values are low by about 0.3 ± 0.2 eV.) In all systems, the larger $M_nCD_2^+$ values are presumed to correspond to the true thermodynamic values, such that the differences in the thresholds must correspond to a barrier in excess of the endothermicity along the potential energy surface of the primary reactions.

This conjecture has been directly confirmed for reactions of all three atomic cations. Here, examination of the forward and reverse reactions demonstrates that the primary reactions have lower thresholds because there is a barrier for the initial dehydrogenation reaction that exceeds the asymptotic energy of the product ions.[106-108] A similar explanation must undoubtedly hold for larger clusters. Although the barrier lies in the exit channel for atomic Fe^+, Co^+, and Ni^+ (and probably M_2^+ as well), for larger clusters, the barrier is probably located in the entrance channel corresponding to the CH bond activation step. This conclusion is suggested by the observation that the thresholds for formation of $M_nCD_2^+$ and $M_nCD_4^+$ are the same. Thus, these thresholds must correspond to a rate-limiting transition state leading to both products and cannot correspond to the thermodynamic limit for either channel. The observation that the $M_nCD_4^+$ products have a barrier to their formation shows that they cannot correspond to physisorbed (intact) methane because formation of this species would have no barrier as a result of the long-range ion-induced dipole attractive interactions.

Figure 9 shows the cluster BDEs to the fragments of methane in the case of the iron system.[100,103] Similar results are available for both the cobalt and nickel systems.[101,102] Like the atomic adsorbates, the BDEs can change dramatically with cluster size for smaller clusters, which can be attributed to variations in their electronic and geometric structures. As for the atomic adsorbates, the BDEs reach asymptotic levels for larger cluster sizes. For these molecular

adsorbates, there are no bulk phase values available for comparison, which potentially makes this cluster thermochemistry of value for estimating such properties on bulk-phase surfaces. The reasonableness of the values obtained can be assessed by comparing their relative orders. Specifically, the ratio of the BDEs for the larger clusters is comparable to that expected on the basis of comparing carbon-carbon single, double, and triple bonds. Thus, the M_n^+–D (taken from the reaction with D_2),[103] M_n^+–CD_2, and M_n^+–CD BDEs for large clusters of M = Fe, Co, and Ni correspond nicely to formation of one, two, and three bonds, respectively, Figure 9. In the few cases where a CD_3 BDE could be measured, the values are close to the BDEs of D, consistent with single bond formation for the methyl group to metal clusters. For the carbide adsorbate, BDEs are similar to CD, consistent with triple bond formation. This indicates that the carbon must be on the surface, forming two covalent bonds using its valence p orbitals and a third bond by accepting electrons into the empty p orbital, similar to the bonding in carbon monoxide. In contrast, an interstitial carbon might be expected to form four covalent bonds, inconsistent with our observations.

Ammonia Activation and Bond Energies to NH_x

Because of its lone pair of electrons, ammonia is more reactive than methane with iron cluster cations (the only metal system yet studied with ammonia by GIBMS).[109] In this system, the guided ion beam results can be compared to the reactivity observed using ion cyclotron resonance mass spectrometry (ICR-MS) at thermal energies only.[110] In the ICR studies, formation of the $M_nND_3^+$ adduct is the only exothermic process observed for clusters with $n \geq 5$, whereas Fe_4^+ also dehydrogenates ammonia to form Fe_4NH^+. Our studies are consistent with these observations, however we also see that Fe_3^+ and Fe_5^+ dehydrogenate ammonia at thermal energies, but with much lower efficiencies than Fe_4^+. At higher energies, as for the methane system, reactions with iron clusters disassemble the molecule forming M_nD^+, $M_nND_2^+$, M_nND^+, and M_nN^+ as well as products formed by loss of M from each of these primary species.

Notably all cluster sizes undergo the dehydrogenation reaction at elevated collision energies, with the Fe_n^+ (n = 3 – 5) clusters showing both an exothermic and an endothermic feature in their cross sections. The endothermic feature is similar for all cluster sizes, so the unique behavior of the n = 3 – 5 clusters is the new, exothermic pathway. These endothermic features can be analyzed using the methods described above along with those for the $Fe_{n-1}ND^+$ and $Fe_{n-2}ND^+$ products. The Fe_n^+–ND BDEs obtained from analysis of the latter secondary and tertiary reactions are consistent with one another and 0.95 ± 0.10 eV greater than those suggested by analysis of the primary process. The larger values presumably correspond to the thermodynamic limit for Fe_nND^+ formation, such that the smaller values derived from the primary dehydrogenation reaction indicate that there are barriers to these processes that are essentially independent of cluster size. All clusters have this activated process available to them, but the n = 3 – 5 systems also have the barrierless pathway not observed for smaller and larger clusters. Possible explanations for this low energy process include formation of an alternate product isomer, reaction on a surface of differing spin, concerted D_2 elimination versus sequential deuteride shifts, but theoretical results suggest that a rearrangement of the metal cluster may facilitate the dehydrogenation reaction.[111] These theoretical results suggest that interaction of Fe_4^+ with ammonia induces a transformation of the iron tetramer from a planar rhomboid to a tetrahedral structure, where the latter allows the NH product to bind in a three-fold site on one face. Clusters smaller than n = 3 cannot place the NH in the strongly bound three-fold site, and larger clusters probably prevent the rearrangement because there are more metal-metal bonds to hold the cluster structure more rigidly.

Figure 9 shows the bond energies for Fe_n^+-ND_y derived in this work and compared to Fe_n^+-CD_y. It can be seen that the Fe_n^+-ND_2 BDEs run parallel to the Fe_n^+-D BDEs (taken from the reaction with D_2)[103] from n = 1 – 6, with the former lying an average 0.78 ± 0.13 eV higher. The parallel character is reasonable because both adsorbates can form a single covalent bond, with the fluctuations reflecting changes in the electronic character of the clusters. The Fe_n^+-ND_2 bonds are stronger because the nitrogen lone pair of electrons donates back to the metal cluster

cation, forming an additional dative bond. It appears that the Fe_n^+-ND_2 BDEs have reached their asymptotic value for n = 6 – 8, 3.25 ± 0.10 eV, 0.65 eV above the asymptotic value for Fe_n^+-D BDEs. As for the O ligands, the asymptotic limit is reached for smaller clusters than for D because the stronger bonding anneals the clusters more readily. Notably, it had previously been assumed that the BDE for NH_2 to iron surfaces equaled that for H atoms,[112-114] however, the present work demonstrates that the electron lone pair on nitrogen is capable of enhancing the bonding for this adsorbate.

A similar effect is observed when comparing ND and CD_2, each of which can form two covalent bonds. Fe_n^+-ND BDEs exceed the Fe_n^+-CD_2 BDEs by 0.5 ± 0.1 eV for $n \geq 6$, which can again be assigned to additional dative bond formation using the lone pair of electrons on nitrogen. For n = 3 – 5, the Fe_n^+-ND BDEs are particularly strong, which is consistent with the ability of these three clusters to dehydrogenate ammonia exothermically. An estimate for the bulk-phase binding energy of ND to iron surfaces is 4.3 eV,[112-114] in the same general range as our values for n = 6 – 10, 13, and 14. Similarly, comparison of Fe_n^+-O and Fe_n^+-ND BDEs shows the former are stronger, even though O, ND, and CD_2 can all form two covalent bonds. As for ND versus CD_2, the difference between O and ND is the number of lone pairs of electrons that can contribute to the bonding.

For the smaller clusters, Fe_n^+-ND_3 BDEs could also be obtained, Figure 9. The variation in these BDEs as a function of n differs from that for Fe_n^+-D, reflecting the one electron donor character of D versus the two electron donor character of ND_3. Thus, the patterns in these two BDEs reflect whether the cluster has a singly occupied valence orbital available for bonding to D versus an empty valence orbital to accept the lone pair of electrons on ammonia.

Conclusion

As detailed above, our gas-phase cluster studies find that atoms (O, H, and C) and molecular fragments (perdeuterated CH, CH_2, NH, NH_2) have BDEs to metal cluster cations that plateau for clusters between about 10 and 20 atoms. This rapid approach to bulk phase

thermodynamics was unexpected, but can be rationalized as a direct consequence of adsorbate chemical bonds being more local phenomena than quantities such as ionization energies and electron affinities, i.e., a small adsorbate can bond directly to only 1 – 4 surface atoms. As long as the cluster is sufficiently large to provide adequate electronic "flexibility", the cluster-adsorbate bond can be as strong as the bulk-adsorbate bond. Our observations that cluster-adsorbate BDEs match the bulk-adsorbate values for O and H atoms on five different metals offers a promise that such well-controlled quantitative gas-phase studies can provide thermodynamic information of use in the evaluation of the mechanisms and energetics of catalytic and surface processes involving a host of reactive adsorbates. Thus, the asymptotic values obtained for molecular adsorbates should be valuable as estimates for surface-adsorbate thermochemistry where little condensed phase data exist for comparison. In general, surface studies are able to measure the binding energies of atomic species (H, O, and N) or the heat of chemisorption of stable molecules (like CO, ethene, water, or ammonia) to surfaces, but there is little experimental information on the thermochemistry of surface species in between these two limits,[115,116] although information on methyl and ethyl groups is available.[117,118] For most molecular fragments, investigators are limited to either theoretical calculations or estimates, for instance, from a bond order conservation – Morse potential (BOC-MP) approach developed by Shustorovich.[119-121] In that regard, it is useful to point out that our BDEs for large iron clusters (Figure 9) are in good agreement with the BOC-MP estimates reported by Bell for the chemisorption enthalpies of H, C, CH, and CH_2 on Fe/W(110) surfaces (where Fe and W surfaces are "closely similar ").[122] Our study is thus one of the first direct experimental validations of this approach for molecular fragments.

Even in the absence of this thermodynamic analogy, clusters may serve as good models for technologically important catalysts that involve highly dispersed metals and for the surface defect sites that are often the active sites for chemistry.[123-127] Clearly, more extensive research is required in both the cluster and surface science fields in order to determine how literally the cluster-surface analogy may be taken and where its limitations lie. However, it is probably just

as interesting to determine when the cluster-surface analogy *fails*, because this opens the possibility of locating specific-sized clusters that may have high chemical reactivity and/or specificity. The strong fluctuations in the cluster-adsorbate BDEs found for smaller clusters are one indication of such a possibility. Another indication is the observation of ammonia activation by Fe_n^+ where $n = 3 – 5$, described above, as well as additional studies by Irion and coworkers who found that Fe_4^+ is unique in its ability to form benzene from smaller hydrocarbons[128] and in its thermal reactivity with ethane.[129] Similarly, Uggerud's group has observed that Co_4^+ and Co_5^+ dehydrogenate methanol at thermal energies, whereas no other cobalt clusters exhibit this reaction.[130] Kondow and coworkers find that only Ni_n^+ ($n = 4 – 6$) release acetylene from benzene,[131] and $M_5O_2^+$ (M = Fe and Co) are particularly active for dehydrogenation of ammonia.[132] Exploration of gas-phase transition metal clusters is also potentially of interest for comparison to tailored catalysts created by deposition of size-selected clusters on a substrate,[1-7,133-136] as such comparisons should provide insight into the influence that cluster-substrate interactions have on the reactivity. Finally, research on gas-phase clusters can play an important role as an interface with theory, both electronic structure theory (at many levels) and dynamics calculations, because clusters are sufficiently small that they can be modeled *directly* by theory, instead of surfaces that are often mimicked by a limited number of atoms. Quantitative experimental results on the reactivity and thermodynamics of clusters thereby provide a benchmark for theory, which can then examine surface chemistry with increased reliability. Examples of this synergy for transition metal species are comparisons of our BDEs for iron, nickel, and vanadium clusters[15,41,48] with calculated values.[137-140] In addition, experimental[105] and theoretical[141,142] reaction rates can be favorably compared for reactions of nickel clusters with H_2.

Acknowledgment. This research was supported by the Chemical Sciences, Geosciences, and Biosciences Division, Office of Basic Energy Sciences, U. S. Department of Energy.

Notes and References

[a] *Department of Chemistry, University of Utah, 315 S. 1400 E. Rm 2020, Salt Lake City, UT, USA. Fax: 01 801-581-8433; Tel: 01-801-581-7885; E-mail: armentrout@chem.utah.edu*

(1) Xu, Z.; Xiao, F.-S.; Purnell, S. K.; Alexeev, O.; Kawi, S.; Deutsch, S. E.; Gates, B. C. *Nature* **1994**, *372*, 346-348.
(2) Heiz, U.; Vanolli, F.; Sanchez, A.; Schneider, W. D. *J. Am. Chem. Soc.* **1998**, *120*, 9668-9671.
(3) Kimble, M. L.; Castleman, A. W.; Mitrić, R.; Bürgel, C.; Bonačić-Koutecký, V. *J. Am. Chem. Soc.* **2004**, *126*, 2526-2535.
(4) Kimble, M. L.; Castleman, A. W. *Int. J. Mass Spectrom.* **2004**, *233*, 99-101.
(5) Lee, S.; Fan, C.; Wu, T.; Anderson, S. L. *J. Am. Chem. Soc.* **2004**, *126*, 5682-5683.
(6) Lee, S.; Fan, C.; Wu, T.; Anderson, S. L. *J. Chem. Phys.* **2005**, *123*, 124710.
(7) Kaden, W. E.; Kunkel, W. A.; Kane, M. D.; Roberts, F. S.; Anderson, S. L. *J. Am. Chem. Soc.* **2010**, *132*, 13097-13099.
(8) Eller, K.; Schwarz, H. *Chem. Rev.* **1991**, *91*, 1121-1177.
(9) *Organometallic Ion Chemistry*; Freiser, B. S., Ed.; Kluwer: Dordrecht, 1996.
(10) Armentrout, P. B. Gas Phase Organometallic Chemistry. In *Topics in Organometallic Chemistry*; Brown, J. M., Hofmann, P., Eds.; Springer-Verlag: Berlin, 1999; Vol. 4; pp 1-45.
(11) Bohme, D. K.; Schwarz, H. *Angew. Chem. Int. Ed.* **2005**, *44*, 2336 – 2354.
(12) Loh, S. K.; Hales, D. A.; Lian, L.; Armentrout, P. B. *J. Chem. Phys.* **1989**, *90*, 5466-5485.
(13) Dietz, T. G.; Duncan, M. A.; Powers, D. E.; Smalley, R. E. *J. Chem. Phys.* **1981**, *74*, 6511-6512.
(14) Loh, S. K.; Hales, D. A.; Armentrout, P. B. *Chem. Phys. Lett.* **1986**, *129*, 527-532.
(15) Lian, L.; Su, C. X.; Armentrout, P. B. *J. Chem. Phys.* **1992**, *97*, 4072-4083.
(16) Lian, L.; Su, C. X.; Armentrout, P. B. *J. Chem. Phys.* **1992**, *97*, 4084-4093.
(17) Hales, D. A.; Su, C.-X.; Lian, L.; Armentrout, P. B. *J. Chem. Phys.* **1994**, *100*, 1049-1057.
(18) Teloy, E.; Gerlich, D. *Chem. Phys.* **1974**, *4*, 417-427.
(19) Ervin, K. M.; Armentrout, P. B. *J. Chem. Phys.* **1985**, *83*, 166-189.
(20) Gerlich, D. *Adv. Chem. Phys.* **1992**, *82*, 1-176.
(21) Daly, N. R. *Rev. Sci. Instrum.* **1960**, *31*, 264-267.
(22) Gioumousis, G.; Stevenson, D. P. *J. Chem. Phys.* **1958**, *29*, 294-299.
(23) Su, T.; Bowers, M. T. Classical Ion-Molecule Collision Theory. In *Gas Phase Ion Chemistry*; Bowers, M. T., Ed.; Academic: New York, 1979; Vol. 1; pp 83-118.
(24) Muntean, F.; Armentrout, P. B. *J. Chem. Phys.* **2001**, *115*, 1213-1228.
(25) Levine, R. D.; Bernstein, R. B. *J. Chem. Phys.* **1972**, *56*, 2281-2287.
(26) Ervin, K. M.; Armentrout, P. B. *J. Chem. Phys.* **1984**, *80*, 2978-2980.
(27) Shvartsburg, A. A.; Ervin, K. M.; Frederick, J. H. *J. Chem. Phys.* **1996**, *104*, 8458-8470.
(28) Chesnavich, W. J.; Bowers, M. T. *J. Phys. Chem.* **1979**, *83*, 900-905.
(29) Armentrout, P. B. Thermochemical Measurements by Guided Ion Beam Mass Spectrometry. In *Adv. Gas Phase Ion Chem.*; Adams, N., Babcock, L. M., Eds.; JAI Press: Greenwich, Connecticut, 1992; Vol. 1; pp 83-119.
(30) Rodgers, M. T.; Ervin, K. M.; Armentrout, P. B. *J. Chem. Phys.* **1997**, *106*, 4499-4508.
(31) Armentrout, P. B. *Int. J. Mass Spectrom. Ion Processes* **2000**, *200*, 219-241.
(32) Armentrout, P. B.; Ervin, K. M.; Rodgers, M. T. *J. Phys. Chem. A* **2008**, *112*, 10071-10085.
(33) Gilbert, R. G.; Smith, S. C. *Theory of Unimolecular and Recombination Reactions*; Blackwell Scientific: London, 1990.
(34) Holbrook, K. A.; Pilling, M. J.; Robertson, S. H. *Unimolecular Reactions*, 2nd ed.; Wiley: New York, 1996.
(35) Truhlar, D. G.; Garrett, B. C.; Klippenstein, S. J. *J. Phys. Chem.* **1996**, *100*, 12771-12800.
(36) Rodgers, M. T.; Armentrout, P. B. *J. Chem. Phys.* **1998**, *109*, 1787-1800.
(37) Koizumi, H.; Armentrout, P. B. *J. Chem. Phys.* **2003**, *119*, 12819-12829.

(38) Armentrout, P. B. *J. Chem. Phys.* **2007**, *126*, 234302.
(39) Aristov, N.; Armentrout, P. B. *J. Phys. Chem.* **1986**, *90*, 5135-5140.
(40) Hales, D. A.; Armentrout, P. B. *J. Cluster Science* **1990**, *1*, 127-142.
(41) Su, C.-X.; Hales, D. A.; Armentrout, P. B. *J. Chem. Phys.* **1993**, *99*, 6613-6623.
(42) Su, C. X.; Hales, D. A.; Armentrout, P. B. *Chem. Phys. Lett.* **1993**, *201*, 199-204.
(43) Su, C. X.; Armentrout, P. B. *J. Chem. Phys.* **1993**, *99*, 6506-6516.
(44) Ervin, K.; Loh, S. K.; Aristov, N.; Armentrout, P. B. *J. Phys. Chem.* **1983**, *87*, 3593-3596.
(45) Armentrout, P. B. "Transition Metal Cluster Ion Chemistry"; Laser Applications in Chemistry and Biophysics, 1986.
(46) Loh, S. K.; Lian, L.; Hales, D. A.; Armentrout, P. B. *J. Phys. Chem.* **1988**, *92*, 4009-4012.
(47) Lian, L.; Su, C. X.; Armentrout, P. B. *Chem. Phys. Lett.* **1991**, *180*, 168-172.
(48) Lian, L.; Su, C.-X.; Armentrout, P. B. *J. Chem. Phys.* **1992**, *96*, 7542-7554.
(49) Lian, L.; Schultz, R. H.; Armentrout, P. B., unpublished results.
(50) Hales, D. A.; Lian, L.; Armentrout, P. B. *Int. J. Mass Spectrom. Ion Processes* **1990**, *102*, 269-301.
(51) Loh, S. K.; Lian, L.; Armentrout, P. B. *J. Am. Chem. Soc.* **1989**, *111*, 3167-3176.
(52) Hales, D. A. Cid of Transition Metal Cluster Ions, University of California, Berkeley, 1990.
(53) Armentrout, P. B.; Hales, D. A.; Lian, L. Collision-Induced Dissociation of Transition Metal Cluster Ions. In *Advances in Metal and Semiconductor Clusters*; Duncan, M. A., Ed.; JAI: Greenwich, 1994; Vol. 2; pp 1-39.
(54) Armentrout, P. B. Guided-Ion Beam Studies of Ionic Transition Metal Clusters and Complexes. In *Metal-Ligand Interactions - Structure and Reactivity*; Russo, N., Salahub, D. R., Eds.; Kluwer: Dordrecht, 1996; pp 23-48.
(55) Armentrout, P. B.; Griffin, J. B.; Conceição, J. Thermochemistry and Reactivity of Transition Metal Cluster Ions. In *Progress in Physics of Clusters*; Chuev, G. N., Lakhno, V. D., Nefedov, A. P., Eds.; World Scientific: Singapore, 1999; pp 198-225.
(56) Yang, D. S.; James, A. M.; Rayner, D. M.; Hackett, P. A. *Chem. Phys. Lett.* **1994**, *231*, 177-182.
(57) Yang, D. S.; James, A. M.; Rayner, D. M.; Hackett, P. A. *J. Chem. Phys.* **1995**, *102*, 3129-3135.
(58) Knickelbein, M. B. *Phys. Rev. A* **2003**, *67*, 013202.
(59) Yang, S.; Knickelbein, M. B. *J. Chem. Phys.* **1990**, *93*, 1533-1540.
(60) Rohlfing, E. A.; Cox, D. M.; Kaldor, A. *Chem. Phys. Lett.* **1983**, *99*, 161-166.
(61) Rohlfing, E. A.; Cox, D. M.; Kaldor, A.; Johnson, K. H. J. C. P. *J. Chem. Phys.* **1984**, *81*, 3846-3852.
(62) Parks, E. K.; Klots, T. D.; Riley, S. J. *J. Chem. Phys.* **1990**, *92*, 3813-3827.
(63) Knickelbein, M. B.; Yang, S.; Riley, S. J. *J. Chem. Phys.* **1990**, *93*, 94-105.
(64) Knickelbein, M. B.; Yang, S. *J. Chem. Phys.* **1990**, *93*, 5760-5768.
(65) Parks, E. K.; Weiller, B. H.; Bechtold, P. S.; Hoffman, W. F.; Nieman, G. C.; Pobo, L. G.; Riley, S. J. *J. Chem. Phys.* **1988**, *88*, 1622-1633.
(66) Miedema, A. R. *Z. Metallkunde* **1978**, *69*, 287.
(67) Miedema, A. R. *Faraday Symp. Royal Soc. Chem.* **1980**, *14*, 136-148.
(68) Armentrout, P. B. *Ann. Rev. Phys. Chem.* **2001**, *52*, 423-461.
(69) Armentrout, P. B. *Eur. J. Mass Spectrom.* **2003**, *9*, 531-538.
(70) Griffin, J. B.; Armentrout, P. B. *J. Chem. Phys.* **1997**, *106*, 4448-4462.
(71) Griffin, J. B.; Armentrout, P. B. *J. Chem. Phys.* **1998**, *108*, 8062-8074.
(72) Xu, J.; Rodgers, M. T.; Griffin, J. B.; Armentrout, P. B. *J. Chem. Phys.* **1998**, *108*, 9339-9350.
(73) Liu, F.; Li, F.-X.; Armentrout, P. B. *J. Chem. Phys.* **2005**, *123*, 064304.
(74) Vardhan, D.; Liyanage, R.; Armentrout, P. B. *J. Chem. Phys.* **2003**, *119*, 4166-4178.
(75) Griffin, J. B.; Armentrout, P. B. *J. Chem. Phys.* **1997**, *107*, 5345-5355.
(76) Griffin, J. B.; Armentrout, P. B. *J. Chem. Phys.* **1998**, *108*, 8075-8083.

(77) Benziger, J. B. Thermochemical Methods for Reaction Energetics on Metal Surfaces. In *Metal-Surface Reaction Energetics*; Shustorovich, E., Ed.; VCH: New York, 1991; pp 53-107.
(78) Toyoshima, I.; Somorjai, G. A. *Catal. Rev. Sci. Eng.* **1979**, *19*, 105-159.
(79) Brennan, D.; Hayward, D. O.; Tradnell, B. M. W. *Proc. Roy. Soc.* **1960**, *A256*, 81-105.
(80) Bragg, J.; Tomkins, T. C. *Trans. Faraday Soc.* **1955**, *51*, 1071-1080.
(81) Wedler, G. *Z. Phys. Chem.* **1961**, *27*, 388.
(82) Benziger, J. B.; Preston, R. E. *Surf. Sci.* **1984**, *141*, 567-579.
(83) Brown, W. A.; Kose, R.; King, D. A. *Chem. Rev.* **1998**, *98*, 797-832.
(84) Rao, C. N. R.; Kamath, P. V.; Yashonath, S. *Chem. Phys. Lett.* **1982**, *88*, 13-16.
(85) Ostrovskii, V. E. *Rus. J. Phys. Chem.* **1988**, *62*, 330.
(86) Li, M.; Liu, S.-R.; Armentrout, P. B. *J. Chem. Phys.* **2009**, *131*, 144310.
(87) Krenn, G.; Eibl, C.; Mauritsch, W.; Hebenstreit, E. L. D.; Varga, P.; Winkler, A. *Surf. Sci.* **2000**, *445*, 343-357.
(88) Beutl, M.; Lesnik, J.; Laundgren, E.; Konvicka, C.; Varga, P.; Rendulic, K. D. *Surf. Sci.* **2000**, *447*, 245-258.
(89) Frese, K. W. *Surf. Sci.* **1987**, *182*, 85-97.
(90) Boszo, F.; Ertl, G.; Grunze, M.; Weiss, M. *J. Catal.* **1977**, *49*, 18-41.
(91) Boszo, F.; Ertl, G.; Weiss, M. *J. Catal.* **1977**, *50*, 519-529.
(92) Bridge, M. E.; Comrie, C. M.; Lambert, R. M. *J. Catal.* **1979**, *58*, 28-33.
(93) Ernst, K.-H.; Schwarz, E.; Christmann, K. *J. Chem. Phys.* **1994**, *101*, 5388-5402.
(94) Christmann, K.; Behm, R. J.; Ertl, G.; Hove, M. A. V.; Weinberg, W. H. *J. Chem. Phys.* **1979**, *70*, 4168-4185
(95) Christmann, K.; Schober, O.; Ertl, G.; Neuman, M. *J. Chem. Phys.* **1974**, *60*, 4528-4541.
(96) Lapujoulade, J.; Neil, K. S. *J. Chem. Phys.* **1972**, *57*, 3535-3546.
(97) Tan, L.; Liu, F.; Armentrout, P. B. *J. Chem. Phys.* **2006**, *124*, 084302-084301-084314.
(98) Liu, F.; Li, M.; Tan, L.; Armentrout, P. B. *J. Chem. Phys.* **2008**, *128*, 194313-194311-194312
(99) Stoltze, P.; Nørskov, J. *Phys. Rev. Lett.* **1985**, *55*, 2502-2505.
(100) Liyanage, R.; Zhang, X.-G.; Armentrout, P. B. *J. Chem. Phys.* **2001**, *115*, 9747-9763.
(101) Liu, F.; Zhang, X.-G.; Liyanage, R.; Armentrout, P. B. *J. Chem. Phys.* **2004**, *121*, 10976-10990.
(102) Citir, M.; Liu, F.; Armentrout, P. B. *J. Chem. Phys.* **2009**, *130*, 054309.
(103) Conceição, J.; Loh, S. K.; Lian, L.; Armentrout, P. B. *J. Chem. Phys.* **1996**, *104*, 3976-3988.
(104) Liu, F.; Armentrout, P. B. *J. Chem. Phys.* **2005**, *122*, 194320-194321-194312.
(105) Liu, F.; Liyanage, R.; Armentrout, P. B. *J. Chem. Phys.* **2002**, *117*, 132-141.
(106) Haynes, C. L.; Chen, Y.-M.; Armentrout, P. B. *J. Phys. Chem.* **1996**, *100*, 111-119.
(107) Haynes, C. L.; Chen, Y.-M.; Armentrout, P. B. *J. Phys. Chem.* **1995**, *99*, 9110-9117.
(108) Liu, F.; Zhang, X.-G.; Armentrout, P. B. *Phys. Chem. Chem. Phys.* **2005**, *7*, 1054-1064.
(109) Liyanage, R.; Griffin, J. B.; Armentrout, P. B. *J. Chem. Phys.* **2003**, *119*, 8979-8995.
(110) Irion, M. P.; Schnabel, P. *J. Phys. Chem.* **1991**, *95*, 10596-10599.
(111) Fossan, K. O.; Uggerud, E. *Dalton Trans.* **2004**, 892-897.
(112) Grunze, M.; Boszo, F.; Ertl, G.; Weiss, M. *Appl. Surf. Sci.* **1978**, *1*, 241.
(113) Ertl, G. *Catalysis: Science and Technology*; Springer: Berlin, 1983; Vol. 4.
(114) Ertl, G. *Catal. Rev. - Sci. Eng.* **1980**, *21*, 201.
(115) *Metal-Surface Reaction Energetics*; Shustorovich, E., Ed.; VCH: New York, 1991.
(116) Campbell, C. T.; Lytken, O. *Surf. Sci.* **2009**, *603*, 1365-1372.
(117) Bent, B. E. *Chem. Rev.* **1996**, *96*, 1361-1390.
(118) Zaera, F. *Chem. Rev.* **1995**, *95*, 2651-2693.
(119) Shustorovich, E. *Acct. Chem. Res.* **1988**, *21*, 183-189.
(120) Shustorovich, E. *Adv. Catal.* **1990**, *37*, 101-163.
(121) Zeigarnik, A. V.; Valdes-Perez, R. E.; Pesenti, J. *J. Phys. Chem. B* **2000**, *104*, 997-1008.

(122) Bell, A. T. Relationship of Reaction Energetics to the Mechanism and Kinetics of Heterogeneously Catalyzed Reactions. In *Metal-Surface Reaction Energetics*; Shustorovich, E., Ed.; VCH: New York, 1991; pp 191-227.
(123) Somorjai, G. *Chemistry in Two Dimensions: Surfaces*; Cornell U.: Ithaca, 1981.
(124) Foster, A. J.; Lobo, R. F. *Chem. Soc. Rev.* **2010**, *39*, 4783–4793.
(125) Zambelli, T.; Wintterlin, J.; Trost, J.; Ertl, G. *Science* **1996**, *273*, 1688-1690.
(126) Over, H.; Kim, Y. D.; Seitsonen, A. P.; Wendt, S.; Lundgren, E.; Schmid, M.; Varga, P.; Morgante, A.; Ertl, G. *Science* **2000**, *287*, 1474-1476.
(127) Ozensoy, E.; Min, B. K.; Santra, A. K.; Goodman, D. W. *J. Phys. Chem. B* **2004**, *108*, 4351-4357.
(128) Schnabel, P.; Irion, M. P.; Weil, K. G. *J. Phys. Chem.* **1991**, *95*, 9688-9694.
(129) Irion, M. P.; Schnabel, P. *Ber. Bunsenges. Phys. Chem.* **1992**, *96*, 1101-1103.
(130) Øiestad, A. M. L.; Uggerud, E. *Chem. Phys.* **2000**, *262*, 169-177.
(131) Hanmura, T.; Ichihashi, M.; Kondow, T. *J. Phys. Chem. A* **2002**, *106*, 4525-4528.
(132) Hirabayashi, S.; Ichihashi, M.; Kondow, T. *J. Phys. Chem. A* **2010**, *114*, 13040-13044.
(133) Lee, S.; Fan, C.; Wu, T.; Anderson, S. L. *J. Phys. Chem. B* **2004**, *109*, 381-388.
(134) Lee, S.; Fan, C.; Wu, T.; Anderson, S. L. *J. Phys. Chem. B* **2005**, *109*, 11340-11347.
(135) Wu, T.; Kaden, W. E.; Anderson, S. L. *J. Phys. Chem. C* **2008**, *112*, 9006-9015.
(136) Kunz, S.; Schweinberger, F. F.; Habibpour, V.; Rottgen, M.; Harding, C.; Arenz, M.; Heiz, U. *J. Phys. Chem. C* **2009**, *114*, 1651-1654.
(137) Stave, M. S.; DePristo, A. E. *J. Chem. Phys.* **1992**, *97*, 3386-3399.
(138) Gronbeck, H.; Rosen, A. *J. Chem. Phys.* **1997**, *107*, 10620-10625.
(139) Wu, X.; Ray, A. K. *J. Chem. Phys.* **1999**, *110*, 2437-2445.
(140) Cervantes-Salguero, K.; Seminario, J. M. *J. Molec. Model.* **2012**, *18*, 4043-4052.
(141) Durmuş, P.; Böyükata, M.; Özçelik, S.; Güvenç, Z. B.; Jellinek, J. *Surf. Sci.* **2000**, *454-456*, 310-315.
(142) Böyükata, M.; Güvenç, Z. B.; Özçelik, S.; Durmuş, P.; Jellinek, J. *Int. J. Quantum Chem.* **2001**, *84*, 208-215.
(143) Liyanage, R.; Conceição, J.; Armentrout, P. B. *J. Chem. Phys.* **2002**, *116*, 936-945.
(144) Conceição, J.; Liyanage, R.; Armentrout, P. B. *Chem. Phys.* **2000**, *262*, 115-130.

Figure Captions

Figure 1. Cross sections for collision-induced dissociation of Ti_4^+ and V_4^+ with Xe as a function of collision energy in the center-of-mass (lower *x* axis) and laboratory (upper *x* axis) frames. Data reproduced from refs. [16,41].

Figure 2. Bond energies (eV) for M_{n-1}^+–M where M = Ti, V, and Cr as a function of cluster size (*n*). Data taken from refs. [16 41,43].

Figure 3. Experimental cohesive energies of Ti, V, Cr, Fe, Co, Ni, and Nb (symbols) normalized by the respective bulk-phase enthalpies of vaporization. Lines show the spherical drop model, eqn (8), for Fe, Ni, and Nb (bottom to top). Data taken from refs. [15-17,41,43,48,50].

Figure 4. Cross sections for the reactions of V_{10}^+ with O2 as a function of collision energy in the center-of-mass (lower *x* axis) and laboratory (upper *x* axis) frames. $V_nO_2^+$ and V_nO^+ products are indicated by closed and open symbols, respectively. σtot is the sum of all products. Data reproduced from ref. [72].

Figure 5. Bond energies (eV) for M_n^+–O where M = V, Cr, Fe, Co, and Ni as a function of cluster size (*n*) normalized to the respective bulk-phase adsorption energy (dashed line). Data taken from refs. [70-76].

Figure 6. Cross sections for the reactions of V_{10}^+ with D_2 as a function of collision energy in the center-of-mass (lower *x* axis) and laboratory (upper *x* axis) frames. Data reproduced from ref. [143].

Figure 7. Bond energies (eV) for M_n^+–D where M = V, Cr, Fe, Co, and Ni as a function of cluster size (*n*) normalized to the respective bulk-phase adsorption energy (dashed line). Data taken from refs. [103-105,143,144].

Figure 8. Bond energies (eV) for M_n^+–N where M = Fe and Co as a function of cluster size (*n*) normalized to the respective bulk-phase adsorption energy (dashed line). Data taken from refs. [97,98].

Figure 9. Comparison of bond energies for Fe_n^+-L where L = D (ref. [103]), C, CD, CD_2 (ref. [100]), ND, ND_2, and ND_3 (ref. [109]). The bulk phase value for iron surfaces binding D is shown by the bar to the right. Bars above this are multiplied by the ratio expected for single, double, and triple bonds from C_2H_y species where y = 6, 4, and 2.

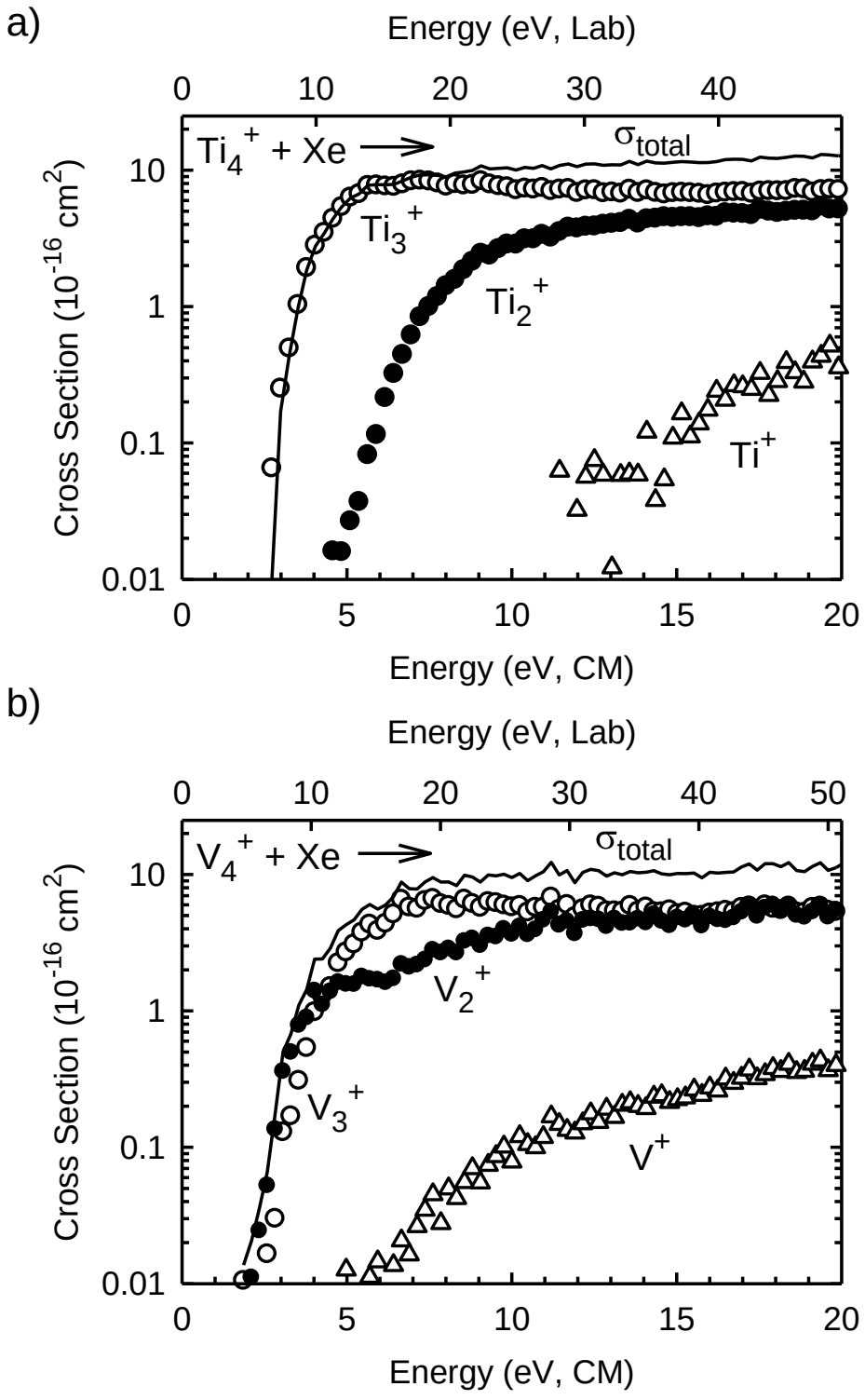
a)
Energy (eV, Lab)
0
10
20
30
40
Ti4+ + Xe
σtotal
Ti3+
Ti2+
Ti+
Cross Section (10-16 cm2)
10
1
0.1
0.01
0
5
10
15
20
Energy (eV, CM)
b)
Energy (eV, Lab)
0
10
20
30
40
50
V4+ + Xe
σtotal
V2+
V3+
V+
Cross Section (10-16 cm2)
10
1
0.1
0.01
0
5
10
15
20
Energy (eV, CM)

Figure 1

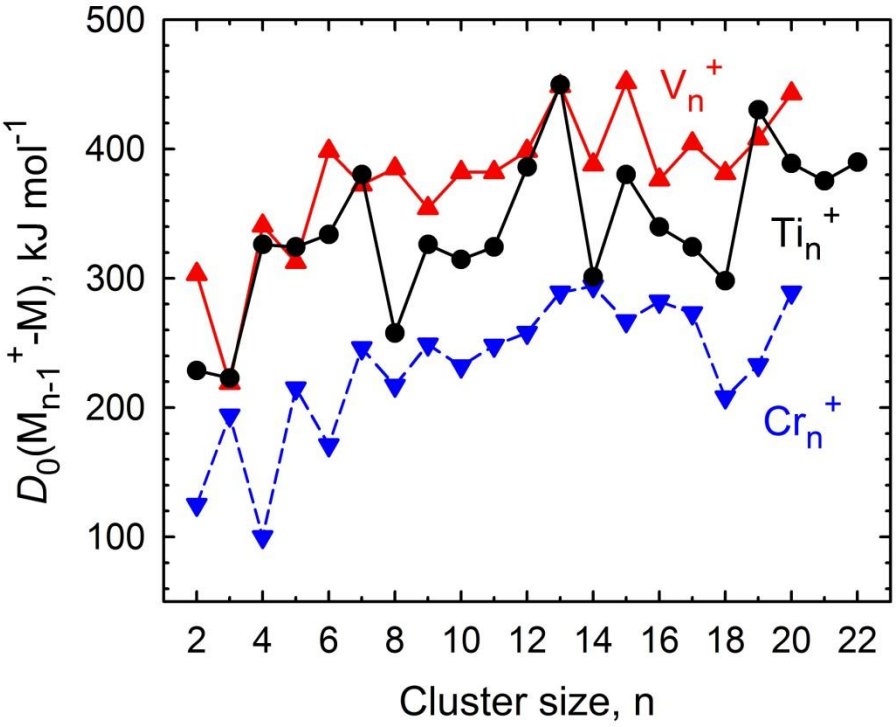

Figure 2

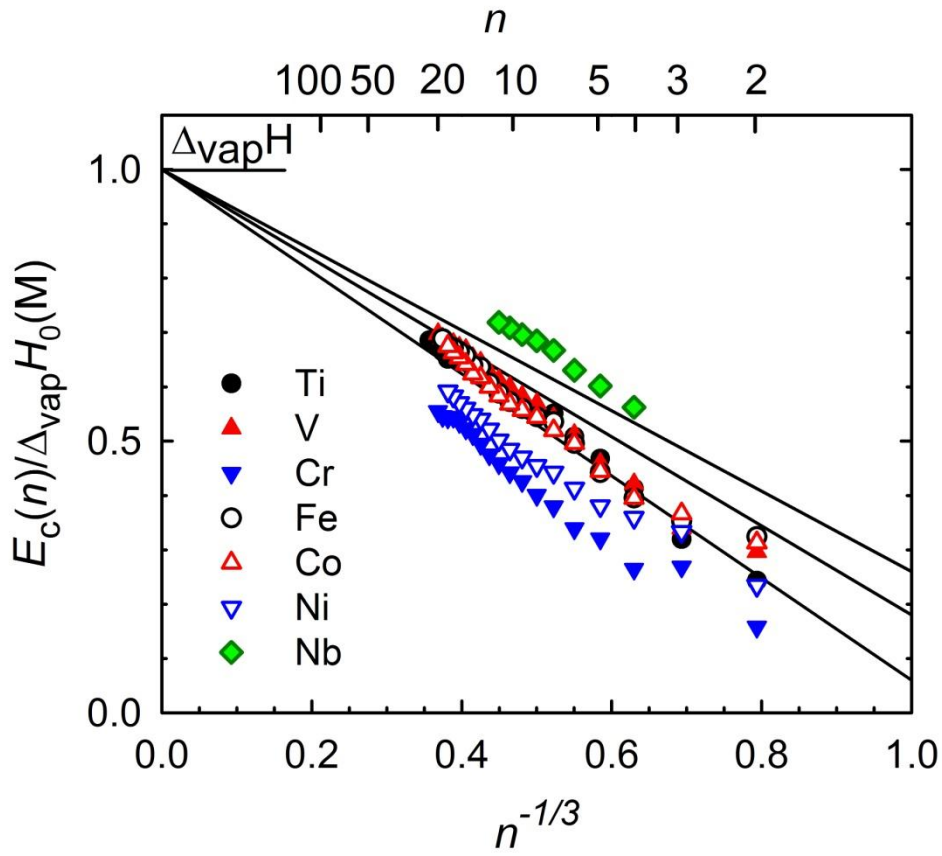

Figure 3

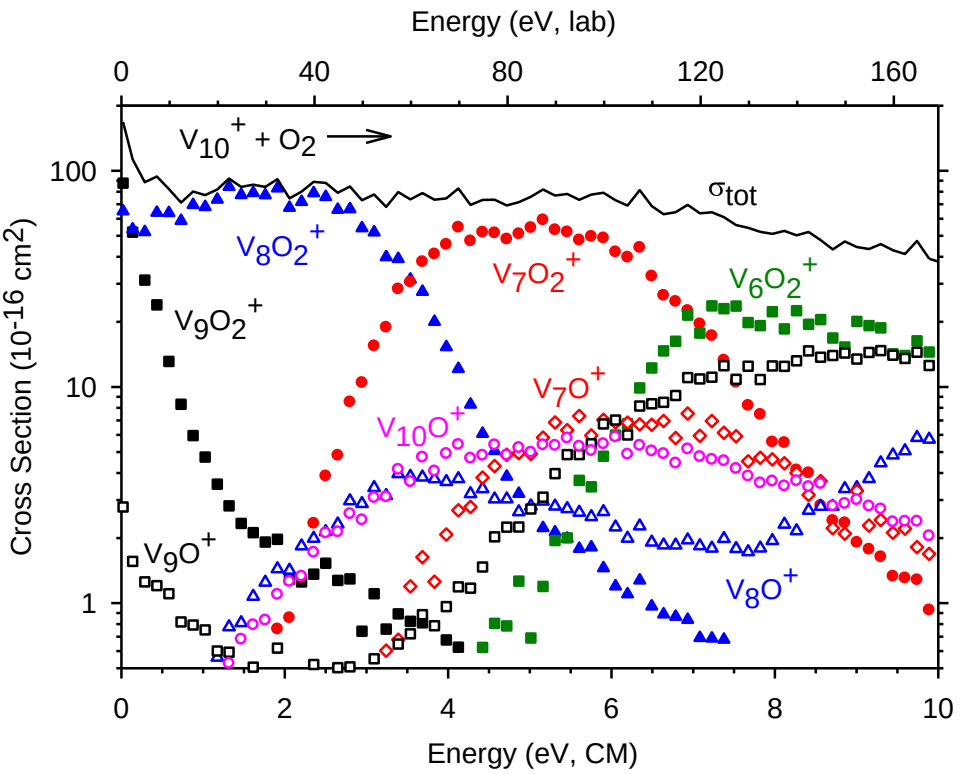

Figure 4

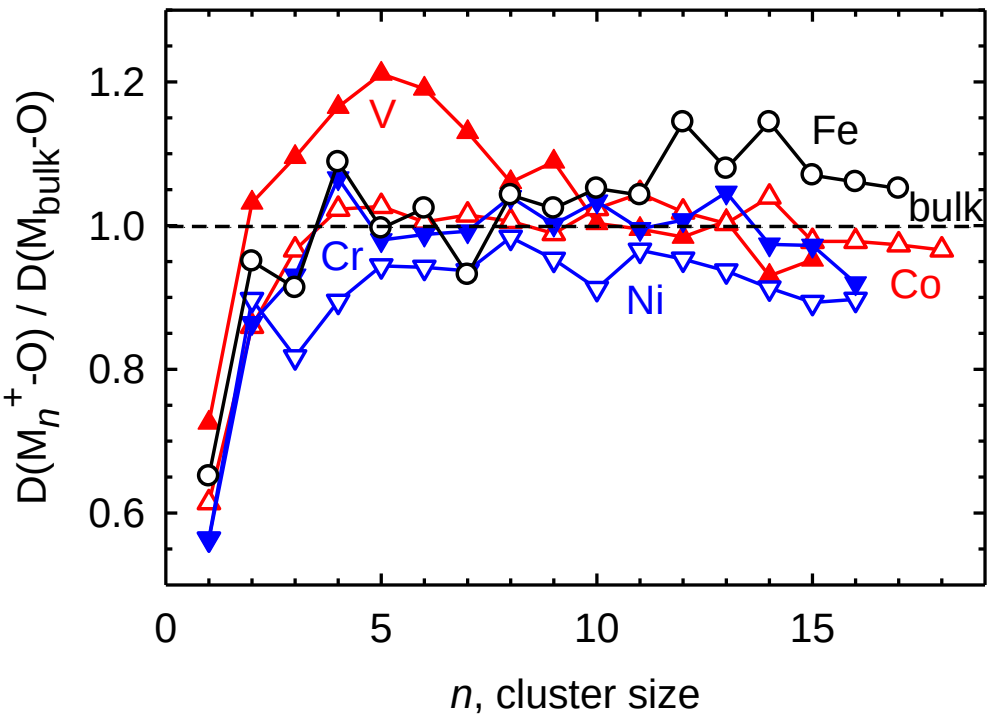

Figure 5

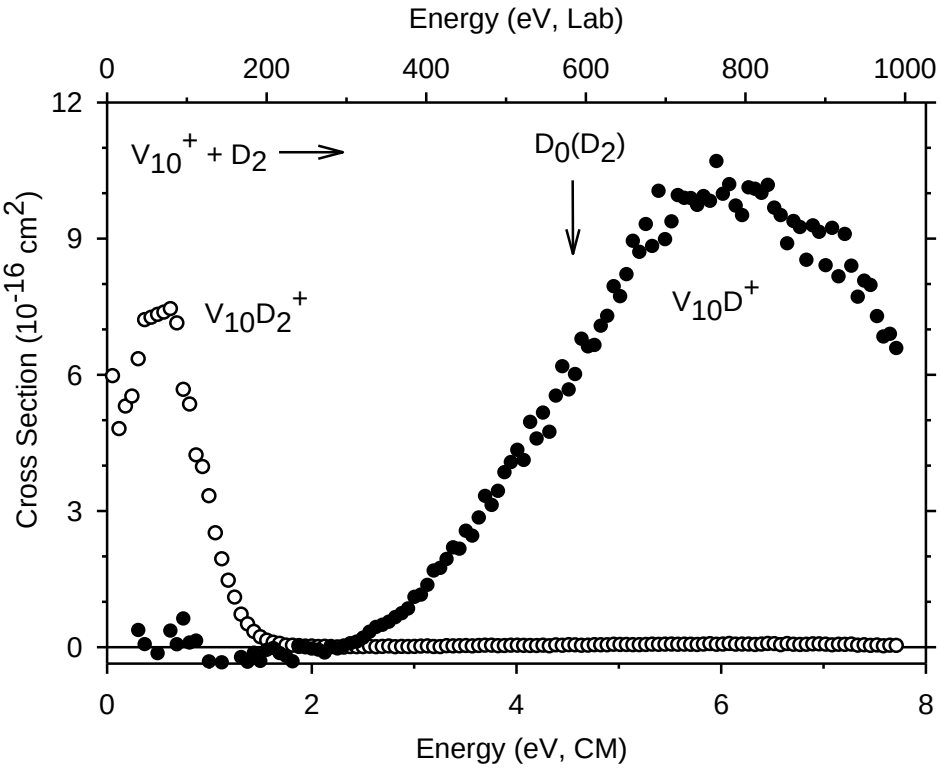

Figure 6

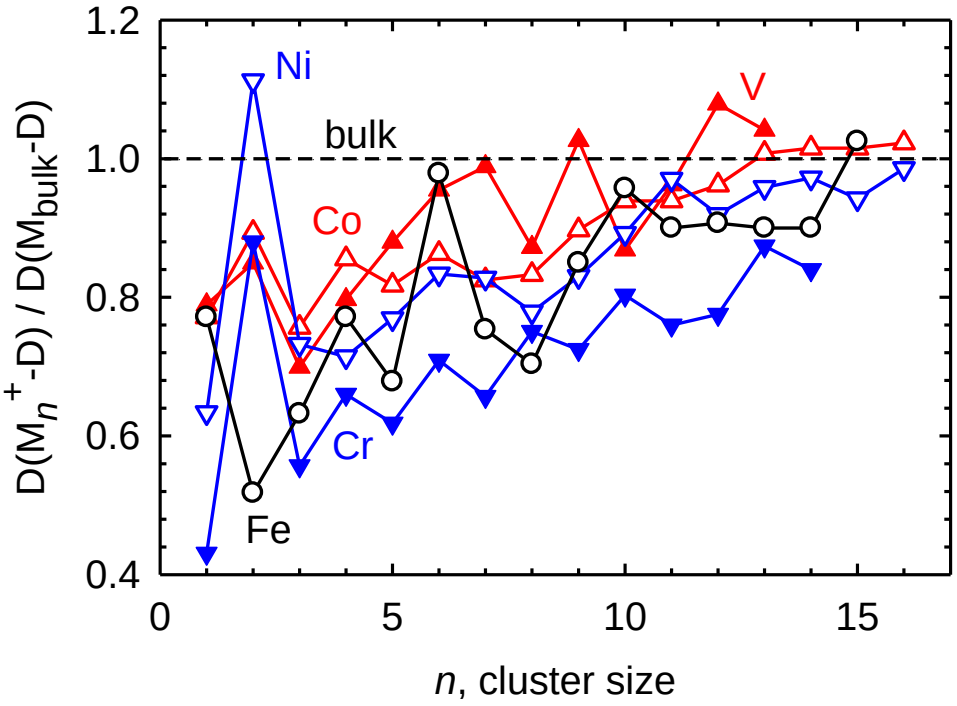

Figure 7

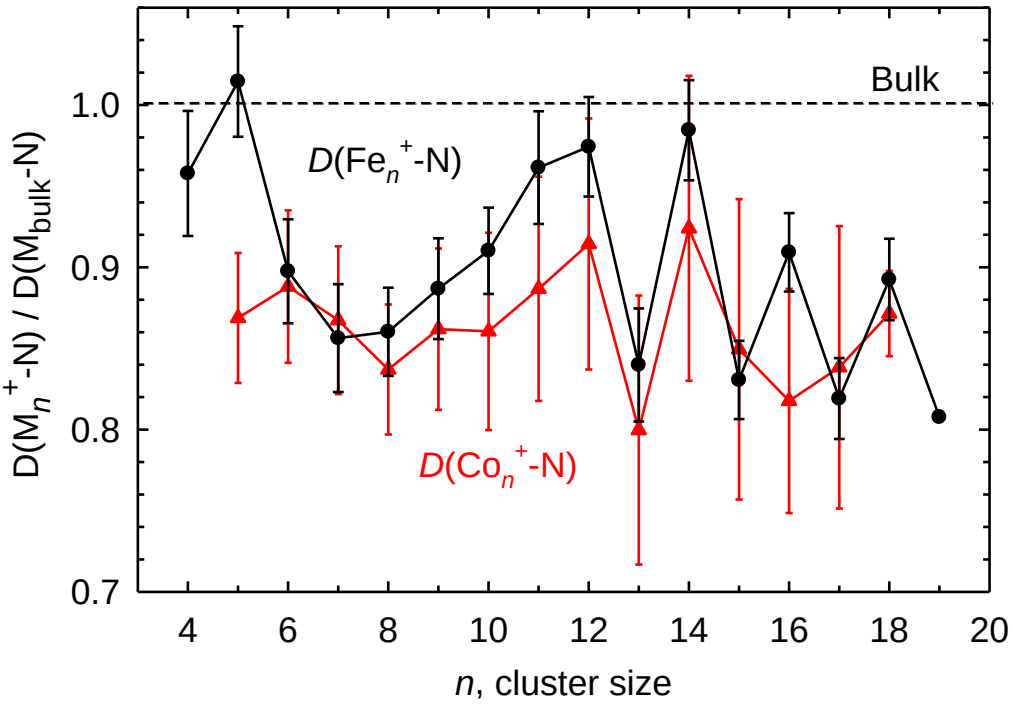

Figure 8

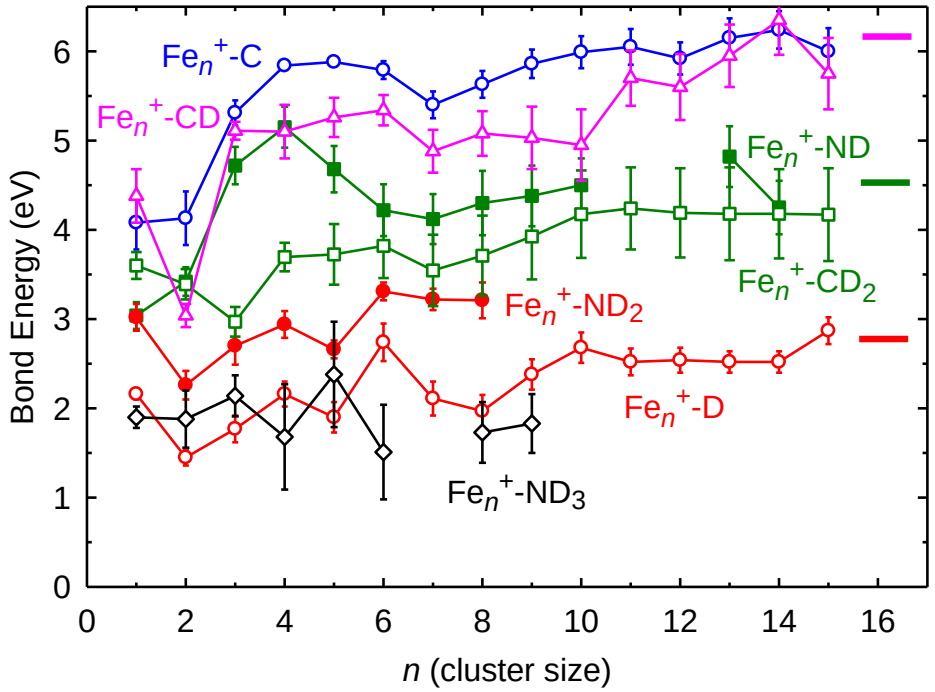

Figure 9